Structure of the human activating natural cytotoxicity receptor NKp30 bound to its tumor cell ligand B7-H6

Yili Li,[1,2] Qian Wang,[1,2] and Roy A. Mariuzza[1,2]

[1]W.M. Keck Laboratory for Structural Biology, University of Maryland Institute for Bioscience and Biotechnology Research, Rockville, MD 20850
[2]Department of Cell Biology and Molecular Genetics, University of Maryland, College Park, MD 20742

The Journal of Experimental Medicine

Natural killer (NK) cells are lymphocytes of the innate immune system that participate in the elimination of tumor cells. In humans, the activating natural cytotoxicity receptors (NCRs) NKp30, NKp44, and NKp46 play a major role in NK cell–mediated tumor cell lysis. NKp30 recognizes B7-H6, a member of the B7 family which is expressed on tumor, but not healthy, cells. To understand the basis for tumor surveillance by NCRs, we determined the structure of NKp30, a member of the CD28 family which includes CTLA-4 and PD-1, in complex with B7-H6. The overall organization of the NKp30–B7-H6–activating complex differs considerably from those of the CTLA-4–B7 and PD-1–PD-L T cell inhibitory complexes. Whereas CTLA-4 and PD-1 use only the front β-sheet of their Ig-like domain to bind ligands, NKp30 uses both front and back β-sheets, resulting in engagement of B7-H6 via the side, as well as face, of the β-sandwich. Moreover, B7-H6 contacts NKp30 through the complementarity-determining region (CDR)–like loops of its V-like domain in an antibody-like interaction that is not observed for B7 or PD-L. This first structure of an NCR bound to ligand provides a template for designing molecules to stimulate NKp30-mediated cytolytic activity for tumor immunotherapy.

CORRESPONDENCE
Roy A. Mariuzza:
rmariuzz@umd.edu

Abbreviations used: CDR, complementarity-determining region; KIR, killer immunoglobulin-like receptor; NCR, natural cytotoxicity receptor; r.m.s., root mean squared; SPR, surface plasmon resonance.

NK cells are a fundamental component of innate immunity against tumors and virally infected cells. The cytolytic activity of NK cells is regulated by a dynamic interplay between activating and inhibitory signals transmitted by distinct classes of receptors found on their surface (Yokoyama and Plougastel, 2003; Bryceson and Long, 2008; Lanier, 2008). The dominant signal received by an NK cell through its interaction with normal numbers of MHC class I molecules on target cells is inhibitory. If the number of MHC class I molecules is reduced through tumorigenic or infectious processes, this inhibitory signal is attenuated and the NK cell is activated. Inhibitory receptors specific for MHC class I include the killer immunoglobulin-like receptors (KIRs) in humans, members of the Ly49 family in rodents, and CD94–NKG2A (Natarajan et al., 2002; Deng and Mariuzza, 2006).

The discovery of activating NK cell receptors, including NKG2D, DNAM-1, 2B4, and the natural cytotoxicity receptors (NCRs), revealed that, in addition to an absent inhibitory signal, activating signals are also required for NK cell triggering and tumor cell lysis (Moretta et al., 2001; Bryceson and Long, 2008; Lanier, 2008). The NCR family includes NKp46 (NCR1 and CD335), NKp44 (NCR2 and CD336), and NKp30 (NCR3 and CD337). In humans, NKp46 is encoded in the leukocyte receptor complex, whereas NKp44 and NKp30 are encoded in the class III region of the MHC locus (Moretta et al., 2001). In the mouse, only the gene for NKp46 is present, with the genes for the other NCRs being absent (NKp44) or a pseudogene (NKp30). These very potent activating receptors are type I transmembrane glycoproteins comprising one (NKp44 and NKp30) or two (NKp46) Ig-like extracellular domains (Moretta et al., 2001, 2006). In a manner reminiscent of T, B, and Fc receptors, NCRs contain charged residues in their transmembrane regions for association

The Rockefeller University Press $30.00
J. Exp. Med. Vol. 208 No. 4 703-714
www.jem.org/cgi/doi/10.1084/jem.20102548

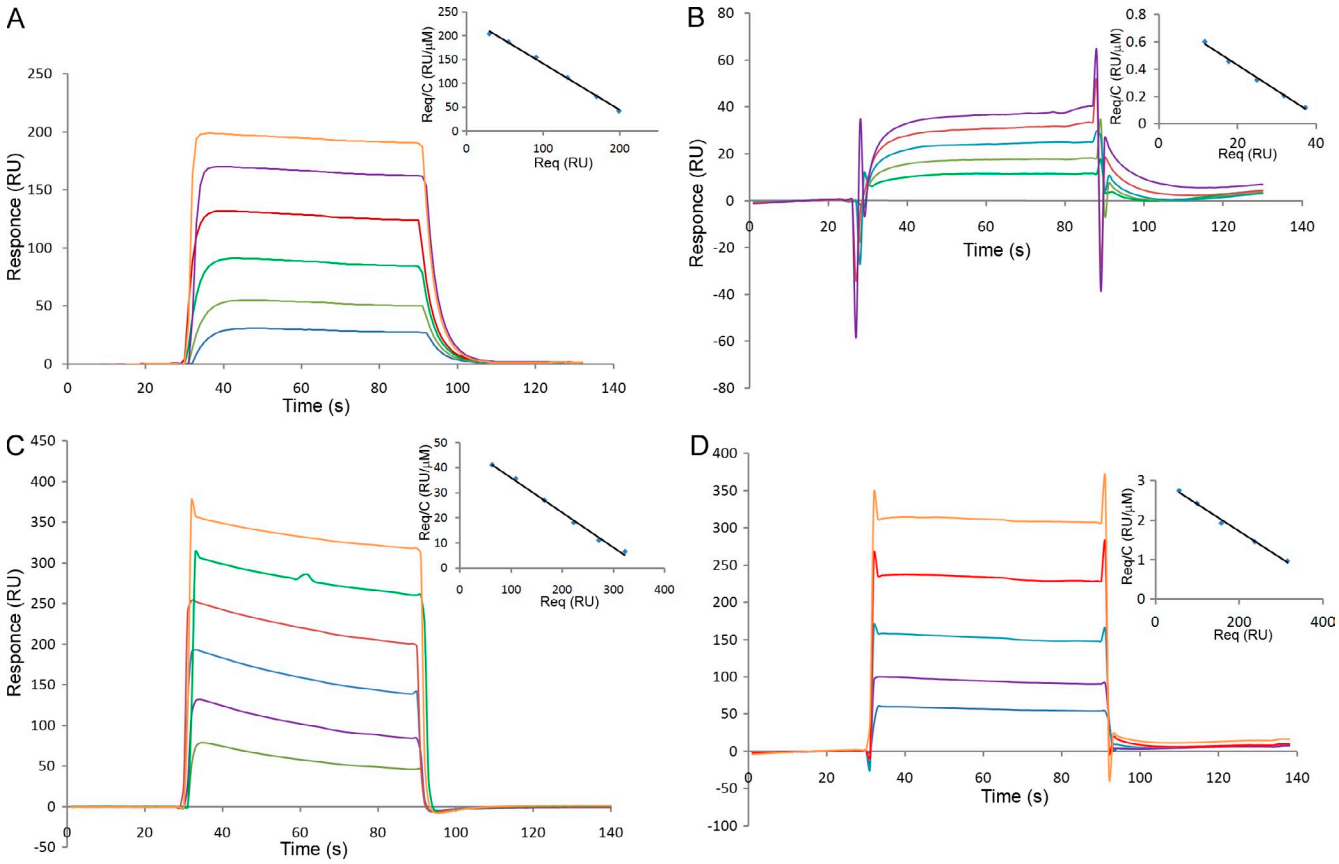

Figure 1. Equilibrium binding of wild-type NKp30 and mutant versions to B7-H6. SPR sensograms for the interaction of wild-type NKp30 (4.7, 2.4, 1.2, 0.59, 0.29, and 0.15 μM; A), NKp30 F85A/L86A mutant (310, 155, 78, 39, and 19 μM; B), NKp30 I50A/S52A mutant (110, 56, 28, 14, 7.0, and 3.5 μM; C), and NKp30 S52R mutant (326, 163, 81, 41, and 20 μM; D) with immobilized B7-H6 (200–1000 RU). K_Ds were calculated from Scatchard plots (insets), after correction for nonspecific binding, by measuring the concentration of free reactants and complex at equilibrium. R_{eq} is the corrected equilibrium response at a given concentration C. $K_D = 1.0 \pm 0.2 \times 10^{-6}$ M for wild-type NKp30; $5.3 \pm 2.0 \times 10^{-5}$ M for F85A/L86A; $1.4 \pm 0.3 \times 10^{-5}$ M for I50A/S52A; $1.5 \pm 0.4 \times 10^{-4}$ M for S52R. The experiments were independently performed at least twice with similar results.

with ITAM-bearing signaling polypeptides: DAP12 for NKp44 and ζ–γ for NKp46 and NKp30 (Bryceson et al., 2006).

Multiple ligands for NKG2D, DNAM-1, and other activating NK cell receptors have been identified (Bottino et al., 2005). In contrast, ligands for the NCR family have been elusive, despite the involvement of NCRs in the lysis of diverse tumor cell lines and primary tumor cells, including neuroblastomas, carcinomas, and lymphoblastic and myeloid leukemias (Moretta et al., 2001, 2006). Recently, however, NKp30 has been shown to bind the nuclear factor BAT3 (Pogge von Strandmann et al., 2007) and the tumor cell surface protein B7-H6 (Brandt et al., 2009). BAT3 is involved in the induction of apoptosis after DNA damage or endoplasmic reticulum stress (Sasaki et al., 2007). As an intracellular protein, BAT3 is not normally expected to be accessible to NKp30. However, heat shock resulted in the appearance of BAT3 on the surface of tumor cells, making it available to bind NKp30 (Pogge von Strandmann et al., 2007). B7-H6 is a new member of the B7 family (Brandt et al., 2009), which includes ligands (B7-1 and B7-2) for the T cell costimulatory receptor CD28 and the coinhibitory receptor CTLA-4, as well as ligands (PD-L1 and PD-L2) for the T cell coinhibitory receptor PD-1 (Zou and Chen, 2008). Like all known B7 family members, B7-H6 comprises two Ig domains with adjacent phase 1 introns in the extracellular region. Importantly, B7-H6 was not detected in normal human tissues but was selectively expressed on a variety of human tumor cell lines, including T and B lymphomas, melanomas, and carcinomas (Brandt et al., 2009). Furthermore, B7-H6 expression on tumor cells triggered NKp30-specific NK cell cytotoxicity and cytokine secretion. Thus, B7-H6 functions as a tumor-induced self-molecule that alerts innate immunity to cellular transformation via its interaction with the activating receptor NKp30 (Brandt et al., 2009). In addition, NKp30 recognizes the tegument pp65 protein of human CMV (Arnon et al., 2005), indicating that NKp30 interacts with multiple ligands, as is the case for the activating NK receptors NKG2D and DNAM-1 (Raulet, 2003; Soriani et al., 2009).

To date, crystal structures have been reported for NKp44 and NKp46 in unbound form (Cantoni et al., 2003; Foster et al., 2003) but not for an NCR in complex with a

Table I. Data collection and structure refinement statistics

Data collection	NKp30–B7-H6	B7-H6
Space group	$P2_12_12_1$	$P2_1$
Unit cells (Å, °)	a = 50.9, b = 74.9, c = 125.5	a = 44.3, b = 70.6, c = 53.2, γ = 100.4°
Resolution (Å)[a]	50–2.3 (2.38–2.30)	50–2.0 (2.07–2.00)
Observations	299,606	159,065
Unique reflections	21,751	21,805
Completeness (%)[a]	98.4 (88.2)	100 (99.6)
Mean $I/\sigma(I)$[a]	53.4 (3.3)	58.0 (2.6)
R_{sym} (%)[a,b]	6.5 (48.5)	5.7 (47.6)
Refinement		
Resolution range (Å)	50–2.30	50–2.0
R_{work} (%)[c]	23.9	24.2
R_{free} (%)[c]	28.9	28.9
Protein atoms	2,543	1,665
Carbohydrate atoms	56	70
Water molecules	16	32
r.m.s. deviations from ideality		
Bond lengths (Å)	0.019	0.019
Bond angles (°)	1.99	1.88
Ramachandran statistics (%)		
Favorable	85.5	93.3
Additional	12.7	5.6
Generous	1.4	1.1
Forbidden	0.4	0.0

[a]Values in parentheses are statistics for the highest resolution shells.
[b]$R_{sym} = \Sigma|I_j - <I>|/\Sigma I_j$, where I_j is the intensity of an individual reflection and $<I>$ is the average intensity of that reflection.
[c]$R_{work} = \Sigma||F_o| - |F_c||/\Sigma|F_o|$, where F_c is the calculated structure factor. R_{free} is as for R_{work} but calculated for a randomly selected 5.0% of reflections not included in the refinement.

tumor-derived (or any other) ligand. To obtain atomic-level information on MHC-independent tumor surveillance by the NCR family, we determined the structures of human NKp30 bound to B7-H6 and of B7-H6 in unbound form.

RESULTS

Structure determination

We produced recombinant NKp30 by in vitro folding from bacterial inclusion bodies and B7-H6 by secretion from baculovirus-infected insect cells. Surface plasmon resonance (SPR) was used to demonstrate specific binding of NKp30 to B7-H6, which is characterized by very fast on and off rates (Fig. 1 A). Both rates were too fast to measure reliably. Under equilibrium binding conditions, a dissociation constant (K_D) of $1.0 \pm 0.2 \times 10^{-6}$ M was obtained, comparable to the affinity of PD-1 for PD-L1 ($K_D = 6 \times 10^{-6}$ M; Lázár-Molnár et al., 2008) or of CTLA-4 for B7-1 (4×10^{-7} M; van der Merwe et al., 1997). We determined the structure of unbound B7-H6 to 2.0 Å resolution by molecular replacement using the V-like and C-like domains of human PD-L1 (Lin et al., 2008) as separate search models. The partially refined B7-H6 structure and the human CTLA-4 structure (Schwartz et al., 2001) were used as search models for solving the structure of the NKp30–B7-H6 complex to 2.3 Å resolution (Table I). We first describe the structures of NKp30 and B7-H6 individually and then proceed to the NKp30–B7-H6 complex.

Structure of NKp30

NKp30 is a type I transmembrane glycoprotein composed of a single Ig-like extracellular domain connected by a short stalk region of six residues to a transmembrane segment and cytoplasmic domain (Pende et al., 1999). NKp30 is monomeric in the crystal, in agreement with its behavior as a monomer in size exclusion chromatography (unpublished data) and on the NK cell surface (Pende et al., 1999). The Ig-like domain of NKp30 is a two-layer β-sandwich that exhibits the chain topology found in IgC domains (C1 set; Williams and Barclay, 1988; Fig. 2). The front and back sheets, composed of β-strands GFC and ABED, respectively, are linked by a canonical intersheet disulfide bond (Cys39–Cys107). In addition, NKp30 contains two α-helices (α1 and α2) preceding β-strands D and E, respectively. One of these helices (α1) is unique to NKp30 among Ig-like domains.

A Dali structure homologue search (http://www2.ebi.ac.uk/dali/fssp/) identified the closest homologue of NKp30 as the V-like domain of PD-L1, a ligand for the T cell inhibitory receptor PD-1, with a Z-score of 12.8 (24% sequence identity). Superposition of NKp30 onto PD-L1 resulted in a root mean squared (r.m.s.) difference of 1.8 Å for 101 α-carbon

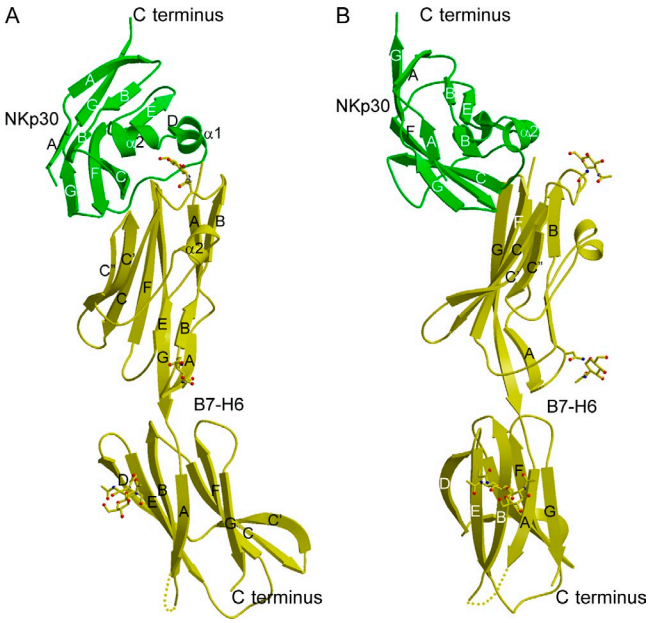

Figure 2. Two views of the NKp30–B7-H6 complex. The strands of the two β-sheets of NKp30 are labeled GFC and ABED. The strands of the two β-sheets of the V-like domain of B7-H6 are labeled GFCC′C′′ and ABE; those of the C-like domain are labeled GFCC′ and ABED. N-linked glycans at B7-H6 residues Asn43 and Asn57 in the V-like domain and Asn208 in the C-like domain are shown in ball-and-stick representation. The view at right is after a rotation of 45° around the vertical axis. The C termini are identified.

atoms. The structural similarity between NKp30 and PD-1 is lower (Z-score = 10.8; 21% sequence identity; r.m.s. difference = 3.1 Å for 101 α-carbon atoms), indicating that NKp30 is more structurally akin to the PD-L1 ligand than to its receptor. NKp30 is considered a member of the CD28 family, which includes PD-1 (CD279), CTLA-4 (CD152), ICOS (CD278), and BTLA (CD272; Brandt et al., 2009). Superposition of NKp30 onto CTLA-4 (Z-score = 10.1; 28% sequence identity) gave an r.m.s. difference of 2.6 Å (95 α-carbon atoms). Thus, NKp30 is clearly more structurally related to PD-1 and CTLA-4 than to adhesion molecules, such as CD2 (Z-score = 9.2 for domain 1; 16% sequence identity) and CD58 (9.2 for domain 1; 16%; Wang et al., 1999), or to the NCRs NKp44 (9.1; 14%; Cantoni et al., 2003) and NKp46 (8.6 for domain 1; 15%; Foster et al., 2003).

Although β-strands GFC in the front sheet and ABE in the back sheet of NKp30 align well with the corresponding strands of PD-1 and CTLA-4, there are large differences on one side of the β-sandwich. Whereas the back sheets of PD-1 and CTLA-4 also include strands C′C′′ or C′, NKp30 lacks these strands and instead contains helices α1 and α2 connected by a short D strand (Fig. 3, A and B). One of these helices (α2) participates in binding B7-H6, as discussed in the next section.

Structure of B7-H6

Like other members of the B7 family, the extracellular portion of B7-H6 is composed of a membrane distal V-like domain and a membrane proximal C-like domain (Fig. 2). B7-H6 behaved as a monomer in solution (unpublished data) and crystallized as a monomer in both free and NKp30-bound forms. B7-H6 and PD-L1 share significant structural similarity, with a Z-score of 16.9 (20% sequence identity) and r.m.s. difference of 2.8 Å (191 α-carbon atoms). The structural similarity between NKp30 and B7-1 is lower but still notable (Z-score = 14.1; 17% sequence identity; r.m.s. difference = 5.3 Å for 177 α-carbon atoms). The two antiparallel β-sheets of the B7-H6 V-like domain are formed by strands GFCC′C′′ and ABE, whereas the β-sandwich of the C-like domain is composed of strands GFCC′ and ABED. B7-H6 contains six potential N-linked glycosylation sites, two in the V-like and four in the C-like domain. In both the free and NKp30-bound B7-H6 structures, clear electron density was visible for carbohydrate chains attached to Asn43 and Asn57 in the V-like domain and to Asn208 in the C-like domain (Fig. S1). The V-like domain of B7-H6 terminates at Val140, which is followed by a three-residue coil (Ala141Ser142Pro143) before the start of β-strand A of the C-like domain (Fig. S2). However, this coil is integral to the C-like domain rather than forming a flexible interdomain linker, as in antibody molecules, which probably helps stabilize the extended, upright stature of B7-H6.

A structure-based sequence alignment of B7-H6 and NKp30 showed several shared secondary structural elements, notably strands ABCEFG and helix α2, which is unique to these two proteins among Ig-like domains (Fig. 3, C and D). Additionally, superposition of B7-H6 onto NKp30 resulted in an r.m.s. difference of 1.7 Å for 81 α-carbon atoms, indicating close similarity. The main differences between these molecules reside on one side of the β-sandwich, where B7-H6 has strands C′C′′ and NKp30 instead has strand D, helix α1, and a long loop connecting strand C and helix α1.

Overview of the NKp30–B7-H6 complex

The structure of the NKp30–B7-H6 complex revealed an assembly with a 1:1 receptor–ligand stoichiometry and a binding interface formed by the front and back β-sheets of the NKp30 C-like domain and the front β-sheet of the B7-H6 V-like domain (Fig. 2). Residues from strands CF and loops BC and FG (front sheet) of NKp30, along with helix α2 (back sheet), juxtapose residues from strands GFCC′ and loops BC, C′C′′, and FG (front sheet) of B7-H6. The overall organization of the NKp30–B7-H6 complex differs considerably from those observed in the PD-1–PDL1 (or PD1–PDL2; Lázár-Molnár et al., 2008; Lin et al., 2008) and CTLA-4–B7-1 (or CTLA-4–B7-2) structures (Schwartz et al., 2001; Stamper et al., 2001). These differences are best appreciated by superposing NKp30 in the NKp30–B7-H6 complex onto PD-1 and CTLA-4 in the PD-1–PD-L and CTLA-4–B7 complexes (Fig. 4, A and B). Compared with NKp30, PD-1 and CTLA-4 engage their ligands at angles of ∼90° and ∼60°, respectively.

The difference in overall complex architecture is explained by two main differences in the binding mode of

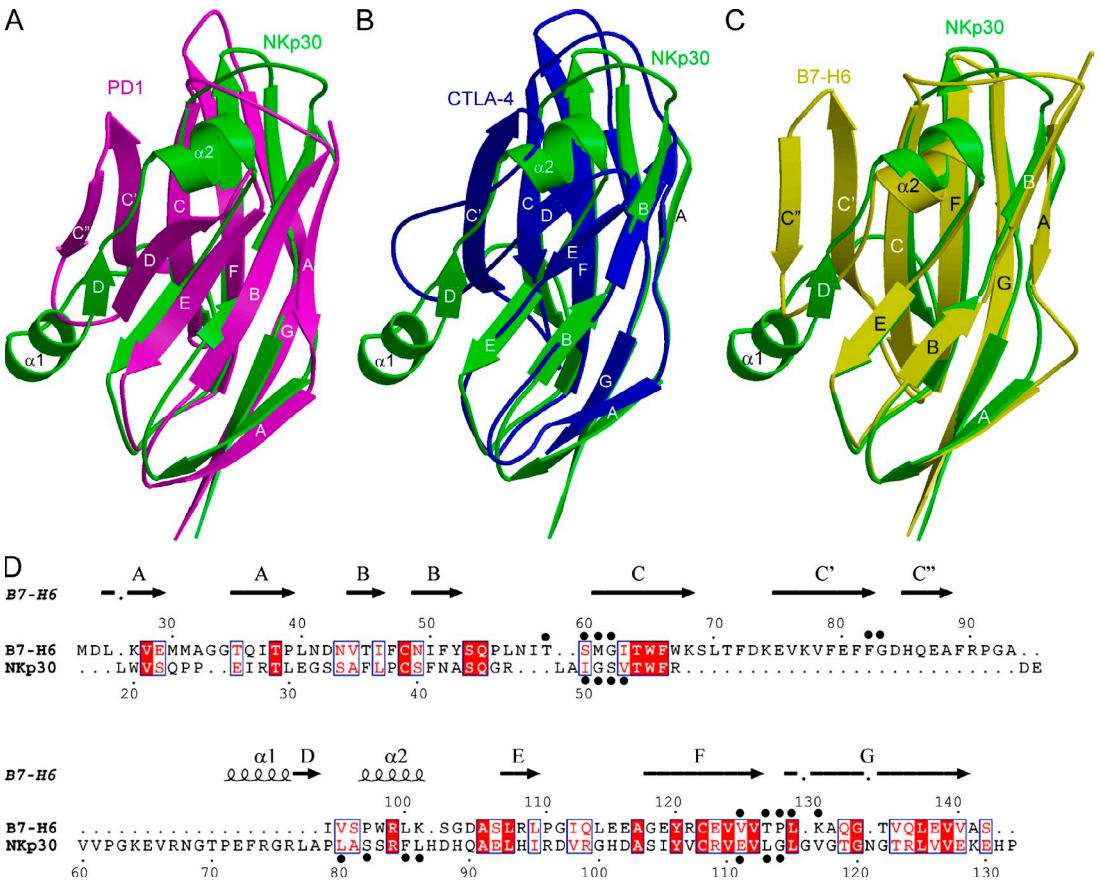

Figure 3. Comparison of NKp30 with PD-1, CTLA-4, and B7-H6. (A) Superposition of the C-like domain of NKp30 (green) onto the V-like domain of PD-1 (magenta; Protein Data Bank accession code 3BIK). (B) Superposition of the C-like domain of NKp30 (green) onto the V-like domain of CTLA-4 (blue; 1IL8). (C) Superposition of the C-like domain of NKp30 (green) onto the V-like domain of B7-H6 (yellow). (D) Structure-based sequence alignment of NKp30 and B7-H6 Ig-like domains. Secondary structure elements are denoted by squiggles (α-helices) and arrows (β-strands). Contacting residues in the NKp30–B7-H6 complex are marked with black dots. White characters on a red background show strictly conserved residues. Residues that are well conserved are drawn in red and framed in blue. The remaining residues are black. Sequence alignments were performed with the program ClustalW (http://www.expasy.ch).

NKp30. First, whereas PD-1 and CTLA-4 use only their front β-sheets to engage the corresponding β-sheets of their ligands in a face-to-face manner (Fig. 4, D and E), the binding site of NKp30 comprises elements from both its front and back β-sheets, resulting in engagement of B7-H6 via the side, as well as face, of the NKp30 β-sandwich (Fig. 4 C). Second, B7-H6 contacts NKp30 in an antibody-like manner (see the next section), with greater involvement by the loops of the V-like domain of the ligand than is the case for PD-L or B7. In the PD-1–PD-L complex, whose interface is dominated by strand-to-strand interactions (Fig. 4 D), the result is a relatively compact structure with an end-to-end distance spanning ∼75 Å, compared with ∼100 Å for the NKp30–B7-H6 complex (Fig. 4 A). However, in the CTLA-4–B7 complex, the involvement by the loops of CTLA-4 in binding ligand, which is greater than in the case of NKp30 (Fig. 4, C and E), results in as extended a structure as the NKp30–B7-H6 complex, with a similar end-to-end distance of ∼100 Å (Fig. 4 B).

The NKp30–B7-H6 interface

In the complex, 12 NKp30 residues contact 11 B7-H6 residues through predominantly hydrophobic interactions, with no bound water molecules in the interface (Fig. 5 A; Table II). The three potential N-linked glycosylation sites of NKp30 are located outside the interface with B7-H6 and so should not interfere with binding. The NKp30–B7-H6 complex buries a total solvent-accessible surface of only 1,130 Å^2, of which 578 Å^2 is contributed by NKp30 and 552 Å^2 by B7-H6. This small interface, which is similar in size to that of the CTLA-4–B7-1 complex (1,250 Å^2) but substantially less than the interface of the PD-1–PDL1 complex (1,900 Å^2), is at the lower limit of the mean value of 1,600 (±400) Å^2 for stable protein–protein complexes (Lo Conte et al., 1999). However, the interface is characterized by high shape complementarity, based on a calculated shape correlation statistic (S_c; Lawrence and Colman, 1993) of 0.77 (S_c = 1.0 for interfaces with geometrically perfect fits), which is at the upper end of the range for protein–protein complexes. This high S_c value is readily

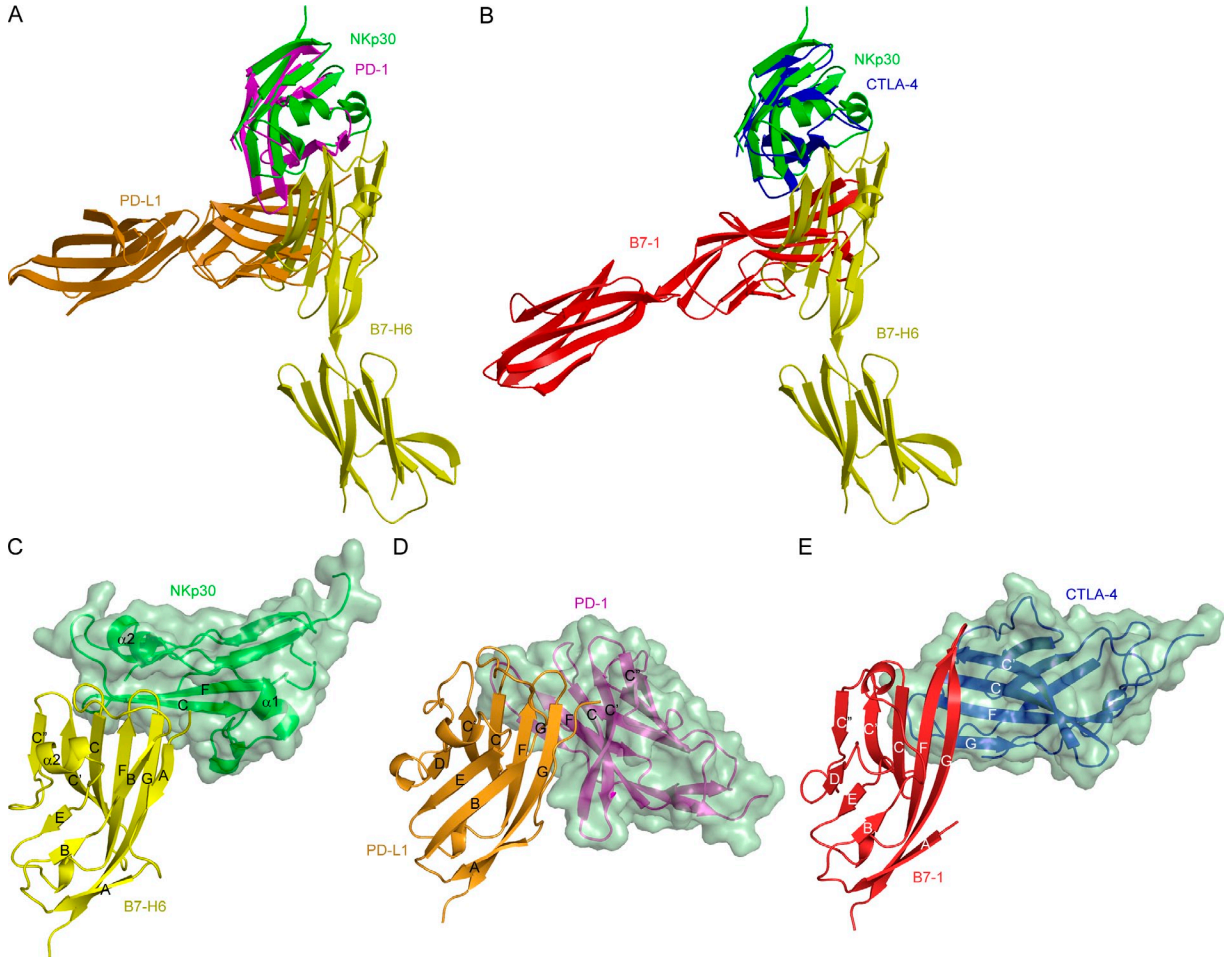

Figure 4. Comparison of the NKp30–B7-H6, PD-1–PD-L1, and CTLA-4–B7-1 complexes. (A) Overlay of the NKp30–B7-H6 and PD-1–PD-L1 complexes by superposing NKp30 (green) onto PD-1 (magenta). B7-H6 is yellow; PD-L1 is orange. (B) Overlay of the NKp30–B7-H6 and CTLA-4–B7-1 complexes by superposing NKp30 (green) onto CTLA-4 (blue). B7-H6 is yellow; B7-1 is red. (C–E) Docking modes in the NKp30–B7-H6, PD-1–PD-L1, and CTLA-4–B7-1 complexes. The three complexes were overlaid by superposing the V-like domains of B7-H6 (yellow), PD1-L1 (orange), and B7-1 (red), and then translated horizontally for viewing.

Table II. Interactions between NKp30 and B7-H6

B7-H6	NKp30		
	Hydrogen bonds[a] and salt bridge[b]	Distance (Å)[c]	Van der Waals contacts
Thr59			Ile50
Ser60			Ile50, Leu86
Met61			Ile50
Gly62			Leu113
Phe82			Leu113, Gly114
Gly83			Ile50
Val125			Ile50, Glu111, Leu113
Thr127	Thr127 Oγ–Gly51 N[a]	3.33	Ile50, Gly51, Ser82, Phe85, Leu86
Pro128	Pro128 O–Val53 N[a]	3.37	Gly51, Ser52, Val53, Leu80, Ser82, Phe85
Leu129			Ser52
Lys130	Lys130 Nζ–Glu111 Oε1[b]	3.09	Ser52, Glu111

[a]Hydrogen bond.
[b]Salt bridge.
[c]Distance indicates length of hydrogen bond or salt bridge.

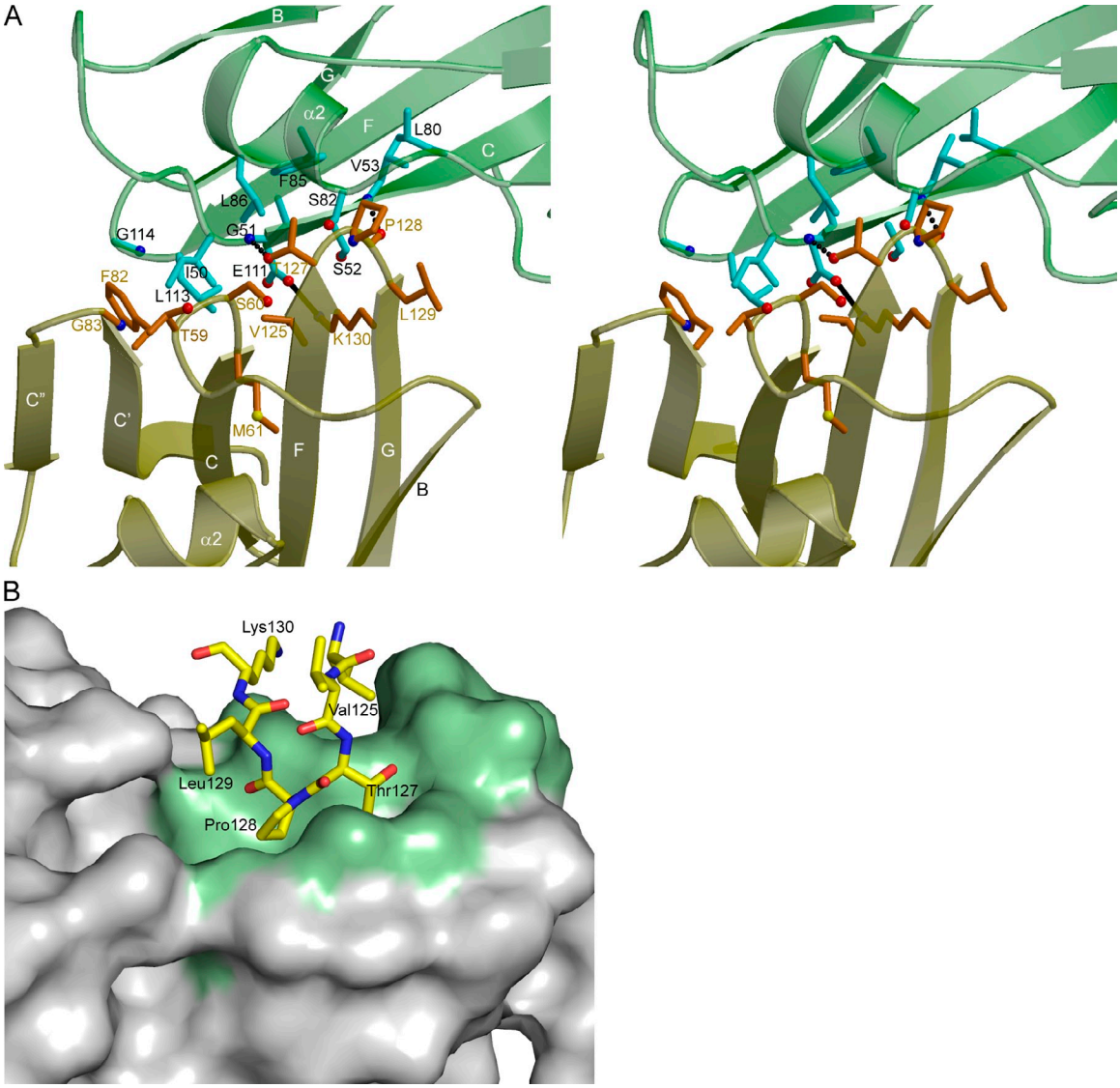

Figure 5. The NKp30–B7-H6 binding interface. (A) Stereo view of the NKp30–B7-H6 interface. The side chains of interacting residues are shown in ball-and-stick representation, with carbon atoms in cyan (NKp30) or orange (B7-H6), nitrogen atoms in blue, and oxygen atoms in red. Hydrogen bonds are drawn as dotted black lines. A salt bridge linking residues NKp30 Glu111 and B7-H6 Lys130 is shown as a solid black line. (B) The NKp30 molecular surface is shown in gray with the region contacting B7-H6 colored green. Residues 125–130 of the B7-H6 FG loop are drawn in stick format and labeled.

explained by the topologies of the contacting surfaces, whereby the FG loop of B7-H6 forms a prominent bulge on the surface of the ligand which fits snugly into a deep groove between strands FG and helix α2 of the NKp30 receptor that is unique to this CD28 family receptor (Fig. 5 B). The high shape complementarity of the NKp30–B7-H6 interface, which is also characterized by the complete exclusion of bulk solvent, probably compensates for its small size to achieve sufficient affinity for NK cell activation.

Residues Thr127 and Pro128 of the FG loop of B7-H6 each make 16 van der Waals contacts with NKp30, which together account for nearly half (44%) the total number of contacts (73) in the complex. These residues bind at the base of groove between strands FG and helix α2 of NKp30 (Fig. 5 B). The only two hydrogen bonds in the interface are formed by these two FG loop residues: B7-H6 Thr127 Oγ–N NKp30 Gly51 and B7-H6 Pro128 O–N NKp30 Val53 (Fig. 5 A; Table II). Notably, the FG loop corresponds to complementarity-determining region (CDR) 3 of antibodies and T cell receptors. Additional contacts are provided by residues from the BC (CDR1-like) and C′C″ (CDR2-like) loops of B7-H6, underscoring an antibody-like interaction with NKp30 which is not evident in the interaction of PD-L or B7 with their receptors (Fig. 4, C–E). In particular, B7-H6 Thr59 and Ser60 (BC loop) engage NKp30 Ile50 (BC loop) and Leu86 (α2 helix) through multiple main chain–main contacts (Fig. 5 A). Overall, the CDR-like loops of B7-H6 contribute 64% of the total contacts to the receptor, compared with 13 and 18%

for CDR-like loops of PD-L1 and B7-1, respectively. The remaining interactions are contributed by strands C′, F, and G, including a salt bridge linking B7-H6 Lys130 (G stand) with NKp30 Glu111 (Fig. 5 A; Table II). On the NKp30 side of the interface, the CDR-like loops of the receptor account for 46% of the total contacts to B7-H6, with helix α2 making a substantial contribution (16%).

To functionally validate the NKp30–B7-H6 interface observed in the crystal structure, we mutated contacting residues of NKp30 in loop BC (Ile50), β-strand C (Ser52), or helix α2 (Phe85, Leu86) and measured binding to B7-H6 by SPR. Mutation of NKp30 Phe85 and Leu86 to alanine reduced affinity for B7-H6 by 53-fold (K_D = 5.3 × 10^{-5} M versus 1.0 × 10^{-6} M for wild-type NKp30; Fig. 1 B). A less pronounced (14-fold), though still significant, effect resulted from alanine substitution of NKp30 Ile50 and Ser52 (Fig. 1 C). Much more disruptive was the replacement of NKp30 Ser52 by arginine (Fig. 1 D), which reduced binding to B7-H6 by 150-fold, thereby confirming the interface identified in the structure.

Conformational changes in B7-H6 upon binding NKp30

Superposition of the V-like domain of free B7-H6 onto the V-like domain of B7-H6 in the complex with NKp30 gave an r.m.s. difference in α-carbon positions of 1.1 Å, indicating close overall similarity (Fig. 6 A). However, strands C′C″ and their associated C′C″ loop have undergone a movement toward NKp30 to optimize interactions with the receptor (Fig. 6 B). In loop C′C″, the side chain of B7-H6 Phe82 is rotated by ∼90° around the Cα–Cβ axis to avoid steric clashes with NKp30 Leu113, and the α-carbon atom of B7-H6 Gly83 is shifted by 2.7 Å toward the receptor to allow formation of van der Waals contacts with NKp30 Ile50 and Leu113. The main chains of loops BC and FG of B7-H6 are each displaced ∼1.6 Å away from NKp30 to avoid steric clashes with the receptor.

In addition to structural adjustments in regions of B7-H6 that contact NKp30, helix α2 of B7-H6 is displaced toward the body of the ligand by a mean of 1.7 Å in the position of its α-carbon atoms (Fig. 6 A). This helix is located on the back sheet of the B7-H6 β-sandwich and opposite the receptor binding site. However, this movement does not appear to be attributable to NKp30 binding but rather to lattice contacts with a neighboring NKp30 molecule in the crystal. Free and bound B7-H6 exhibit nearly identical hinge angles between the V-like and C-like domains, suggesting limited conformational flexibility in the interdomain region that is unrelated to receptor binding. In contrast, the hinge angles of free and bound PD-L1 were found to differ by ∼40° (Lin et al., 2008), indicating substantially greater flexibility that is likely attributable to structural differences in the interdomain regions of PD-L1 and B7-H6.

DISCUSSION

The NKp30–B7-H6 structure revealed that this NK cell activating complex is distinct from the CTLA4–B7 and PD-1–PD-LT cell inhibitory complexes in both overall organization and detailed atomic interactions that mediate binding and specificity. The structure provides the first information on the molecular basis for tumor cell recognition by any member of the NCR family, which includes NKp30, NKp44, and NKp46. In addition, the NKp30–B7-H6 structure establishes certain constraints that must be satisfied by any mechanism proposed to describe signaling through the NKp30 pathway and the integration of these signals into the overall NK cell response.

Upon NK cell–target cell interaction, a highly organized complex of molecules, termed the NK cell immune synapse, is formed at the contact area of both cells (Orange, 2008). These molecules include inhibitory NK receptors that monitor MHC class I expression on target cells (KIRs and Ly49s in human and mouse, respectively), activating NK receptors that recognize MHC-like or non-MHC ligands (NKG2D, DNAM-1, and 2B4), cytoskeletal proteins

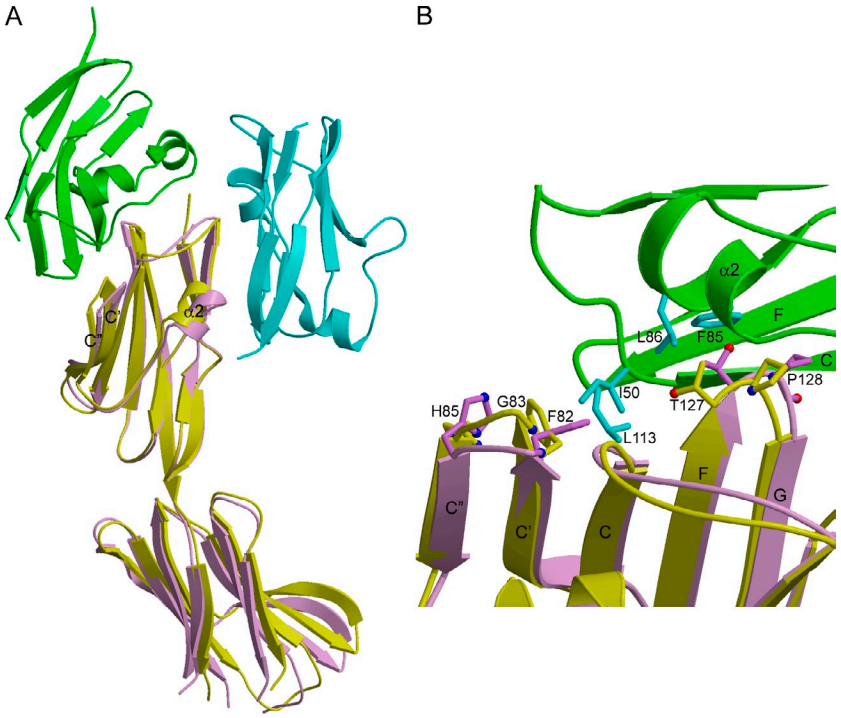

Figure 6. Conformational changes in B7-H6 upon binding NKp30. (A) Comparison of free B7-H6 (violet) and B7-H6 (yellow) in complex with NKp30. The two structures were superposed through the V-like domain of B7-H6. The NKp30 molecule bound to B7-H6 is green; a neighboring NKp30 molecule in the crystal is cyan. (B) Structural rearrangements in B7-H6 induced by binding to NKp30. Bound B7-H6 is yellow; unbound B7-H6 is violet.

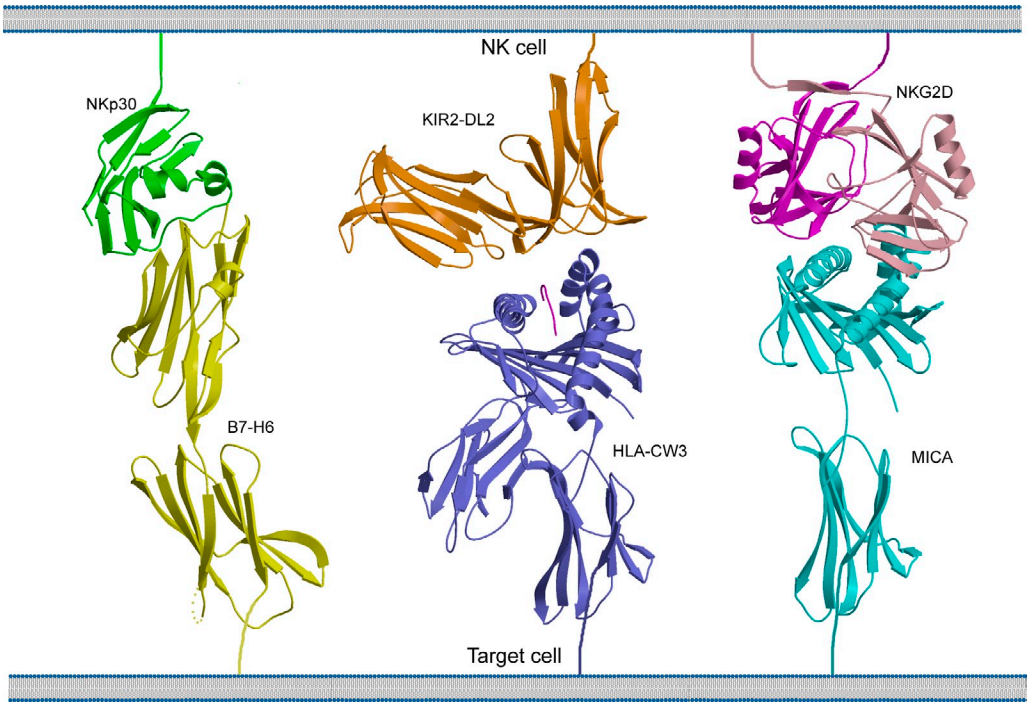

Figure 7. Hypothetical model of interactions at the human NK cell–target cell immune synapse. The distance spanned by the NKp30–B7-H6 complex is comparable to those spanned by the KIR2DL2–HLA-Cw3 (1EFX) and NKG2D–MICA (1HYR) complexes.

(F-actin and tailin), and integrins (CD11a and CD11b; Vyas et al., 2002; Orange, 2008). It has been proposed that the unique compartmentalization of molecules observed at immune synapses is regulated by a sorting mechanism based on molecular dimensions, with relatively small signaling molecules (e.g., NK receptors) localizing to a central zone and larger adhesion molecules (e.g., integrins) residing in the periphery (van der Merwe et al., 2000; Bromley et al., 2001; Orange, 2008). Accordingly, we compared the dimensions of the NKp30–B7-H6 complex with those of the KIR–MHC and NKG2D–MICA complexes (Boyington et al., 2000; Li et al., 2001), both of which accumulate at the NK cell synapse (Davis et al., 1999; McCann et al., 2007; Orange, 2008; Fig. 7). In the NKp30–B7-H6 complex, the distance spanned by the molecules is ~100 Å, which is approximately the distances bridged by the KIR–HLA-C and NKG2D–MICA complexes. This suggests that these receptor–ligand pairs could potentially co-localize with NKp30–B7-H6 in the central zone of the NK cell immune synapse. In addition, tumor cells expressing both MICA and B7-H6 could possibly trigger synergistic activation of NK cells.

An important feature of NKp30 and B7-H6 is their monomeric nature. Whereas CTLA-4 exists as a disulfide-linked homodimer on the T cell surface, NKp30, like PD-1, exists as a monomer in solution, in the crystal, and on the NK cell surface (Pende et al., 1999). In this regard, it should be noted that NKp30 and PD-1 lack the extracellular equivalent of Cys122 in CTLA-4 that forms the intermolecular disulfide in the CTLA-4 homodimer. Similarly, whereas B7, the ligand for CTLA-4, forms noncovalent dimers (Ikemizu et al., 2000), B7-H6 is monomeric both in solution and the crystal. The monomeric state of NKp30 and B7-H6 precludes formation of the type of alternating, periodic assembly observed in CTLA-4–B7 crystal structures, in which bivalent CTLA-4 homodimers bridge bivalent B7 homodimers in the immune synapse (Schwartz et al., 2001; Stamper et al., 2001). Instead, simple diffuse processes probably mediate the engagement NKp30 and B7-H6 in interacting cells and the subsequent accumulation of NKp30–B7-H6 complexes in the central zone of the immune synapse, as proposed for PD-1–PD-L complexes, which are also monomeric (Lázár-Molnár et al., 2008).

Although NKp30 is structurally unrelated to NKG2D, which belongs to the C-type lectin-like superfamily, these two activating NK receptors present several intriguing parallels. Both recognize induced self-molecules expressed on tumor cells that alert innate immunity to cellular transformation: MICA and MICB for NKG2D (Raulet, 2003) and B7-H6 for NKp30 (Brandt et al., 2009). Moreover, both receptors bind multiple ligands. Besides MICA and MICB, human NKG2D interacts with ULBP1–4, whereas mouse NKG2D binds H-6, RAE-1, and MULT1 (Raulet, 2003). Likewise, in addition to B7-H6, NKp30 recognizes the nuclear factor BAT3 (Pogge von Strandmann et al., 2007) and pp65, a human CMV tegument protein (Arnon et al., 2005). However, whereas all NKG2D ligands are structurally related to MHC class I molecules, B7-H6, BAT3, and pp65 appear to be completely unrelated, both in terms of their structure (the proteins lack any sequence homology) and origin (B7-H6 is a cell

surface protein; BAT3 is a nuclear protein released upon heat shock; pp65 is a structural protein of CMV found in the nucleus and cytoplasm of infected cells). In the case of NKG2D, crystallographic studies of NKG2D bound to MICA, ULBP3, and RAE-1 (Li et al., 2001, 2002; Radaev et al., 2001; McFarland et al., 2003) have shown that NKG2D recognizes these MHC-like ligands using a single binding site formed by the two identical subunits of this homodimeric receptor. In addition, only ∼60% of the solvent-accessible surface in the NKG2D–ligand complexes is nonpolar (McFarland et al., 2003), whereas the NKp30–B7-H6 interface is 69% hydrophobic. Whether NKp30 binds BAT3 and pp65 through the same site as B7-H6 is not clear, given the disparate nature of these ligands. It is conceivable that NKp30 may possess distinct, albeit overlapping, binding sites for these molecules, which may comprise residues from both its front and back β-sheets, as seen in the NKp30–B7-H6 complex, or be restricted to residues from the front β-sheet alone, in the manner of the CTLA4–B7 and PD-1–PD-L complexes (Schwartz et al., 2001; Stamper et al., 2001; Lázár-Molnár et al., 2008; Lin et al., 2008).

The availability of the NKp30–B7-H6 structure should accelerate the development of molecules to manipulate the NKp30 pathway for tumor immunotherapy. For example, soluble forms of B7-H6, or compounds designed to mimic the CDR-like loops of B7-H6 that bind NKp30, could be used to augment NK cell responses to tumor cells through induction of NKp30-mediated cytolytic activity. Alternatively, soluble forms of NKp30 fused to antibody Fc regions with effector functions may serve as reagents for eliminating B7-H6–expressing tumor cells via antibody-dependent cell-mediated cytotoxicity. Although such therapeutic applications will likely require structure-based engineering of variants of NKp30 that bind B7-H6 with high affinity (or vice versa), this has been achieved in the case of belatacept (Larsen et al., 2005), a high-affinity mutant of CTLA-4 in clinical trials for preventing rejection in kidney transplantation (Snanoudj et al., 2007).

MATERIALS AND METHODS

Protein production and purification. The extracellular portion of NKp30 (residues Leu19–Gly135) was cloned into the expression vector pET-26b (Novagen) and expressed as inclusion bodies in BL21(DE3) *Escherichia coli* cells (EMD). The inclusion bodies were washed with 50 mM Tris-HCl, pH 8.0, containing 5% (vol/vol) Triton X-100, and then dissolved in 8 M urea, 50 mM Tris-HCl, pH 8.0, and 10 mM DTT. For in vitro folding, the inclusion bodies were diluted into ice-cold folding buffer containing 0.4 M L-arginine–HCl, 50 mM Tris-HCl, pH 8.0, 1 mM EDTA, 3 mM reduced glutathione, and 0.9 mM oxidized glutathione to a final protein concentration of 40 mg/liter. After 72 h at 4°C, folded proteins were separated from aggregates using a Superdex S-75 column (GE Healthcare). Further purification was performed by MonoS chromatography. Mutants of NKp30 were constructed by overlap PCR and expressed in *E. coli* in the same way as the wild-type receptor.

The extracellular portion of B7-H6 (residues Asp25–Ser262) was fused to the gp67 secretion signal sequence of baculovirus expression vector pAcGP67-B (BD) with a C-terminal His_6 tag and expressed in SF9 insect cells (Invitrogen). In a typical preparation, 500 ml Sf9 cells at 1.4×10^6 cells/ml were inoculated with 12 ml of recombinant baculovirus at 1.0×10^8 pfu/cell. Supernatants were harvested 4 d after infection and loaded onto a Ni^{2+}-NTA column (GE Healthcare) for affinity purification. Recombinant B7-H6 was further purified by sequential Superdex S-75 and MonoQ columns.

Crystallization and data collection. Crystals of unbound B7-H6 (10 mg/ml) were grown in hanging drops at room temperature in 0.2 M $LiCl_2$ and 20% (wt/vol) polyethylene glycol (PEG) 3350. For crystallization of the NKp30–B7-H6 complex, 5 mg/ml NKp30 and 10 mg/ml B7-H6 were mixed in a 1:1 volume ratio. The complex crystallized in 20% (wt/vol) PEG 3350 and 0.2 M KF in hanging drops at room temperature.

For data collection, both crystals were transferred to a cryoprotectant solution of mother liquor containing 30% (vol/vol) glycerol, before flash cooling in liquid nitrogen. X-ray diffraction data were collected to 2.0 Å resolution for unbound B7-H6 and to 2.3 Å resolution for the NKp30–B7-H6 complex at beamline X29 of the Brookhaven National Synchrotron Light Source. The B7-H6 crystal belongs to space group $P2_1$ with one molecule per asymmetric unit; the NKp30–B7-H6 crystal belongs to space group $P2_12_12_1$ with one complex molecule per asymmetric unit. All data were indexed, integrated, and scaled with the program HKL2000 (Otwinowski and Minor, 1997). Data collection statistics are summarized in Table I.

Structure determination and refinement. The structure of B7-H6 was solved by molecular replacement with Phaser (Storoni et al., 2004) using the V-like and C-like domains of human PD-L1 (Protein Data Bank accession no. 3BIK; Lin et al., 2008) as separate search models. The partially refined B7-H6 structure and the human CTLA-4 structure (1I85; Schwartz et al., 2001) were used as search models for solving the structure of the NKp30–B7-H6 complex. All refinements were performed using the program CNS1.1 (Brünger et al., 1998), including iterative cycles of simulated annealing, positional refinement, and *B* factor refinement, interspersed with model rebuilding into σ_A-weighted $F_o - F_c$ and $2F_o - F_c$ electron density maps using XtalView (McRee, 1999). Refinement statistics are summarized in Table I. Stereochemical parameters were evaluated with PROCHECK (Laskowski et al., 1993). Atomic coordinates and structure factors for the NKp30–B7-H6 complex and B7-H6 have been deposited in the Protein Data Bank under accession nos. 3PV6 and 3PV7, respectively.

SPR analysis. The interaction of wild-type and mutant NKp30 receptors with B7-H6 was assessed by SPR using a BIAcore T100 biosensor (GE Healthcare). Typically, 200–1,000 resonance units of B7-H6 were immobilized on a CM5 sensor chip by random amine-coupling. Solutions containing different concentrations of NKp30 were injected sequentially over flow cells immobilized with B7-H6 or buffer as a blank. The data were analyzed using BIAevaluation 4.1 software (GE Healthcare). Dissociation constants (K_Ds) were determined from Scatchard analysis, after correction for nonspecific binding, by measuring the concentration of free reactants and complex at equilibrium. Standard deviations for two or more independent K_D determinations were typically <20%.

Online supplemental material. Fig. S1 shows electron density for two *N*-acetylglucosamine residues linked to Asn208 of B7-H6 in the NKp30–B7-H6 complex. Fig. S2 shows the interdomain region of B7-H6. Online supplemental material is available at http://www.jem.org/cgi/content/full/jem.20102548/DC1.

We thank H. Robinson (Brookhaven National Synchrotron Light Source) for x-ray data collection.

This study was supported by the National Institutes of Health grant AI047990. Support for beamline X29 comes from the Offices of Biological and Environmental Research and of Basic Energy Sciences of the US Department of Energy, and from the National Center for Research Resources of the National Institutes of Health.

The authors declare no competing financial interests.

Submitted: 8 December 2010
Accepted: 16 February 2011

REFERENCES

Arnon, T.I., H. Achdout, O. Levi, G. Markel, N. Saleh, G. Katz, R. Gazit, T. Gonen-Gross, J. Hanna, E. Nahari, et al. 2005. Inhibition of the NKp30 activating receptor by pp65 of human cytomegalovirus. *Nat. Immunol.* 6:515–523. doi:10.1038/ni1190

Bottino, C., R. Castriconi, L. Moretta, and A. Moretta. 2005. Cellular ligands of activating NK receptors. *Trends Immunol.* 26:221–226. doi:10.1016/j.it.2005.02.007

Boyington, J.C., S.A. Motyka, P. Schuck, A.G. Brooks, and P.D. Sun. 2000. Crystal structure of an NK cell immunoglobulin-like receptor in complex with its class I MHC ligand. *Nature.* 405:537–543. doi:10.1038/35014520

Brandt, C.S., M. Baratin, E.C. Yi, J. Kennedy, Z. Gao, B. Fox, B. Haldeman, C.D. Ostrander, T. Kaifu, C. Chabannon, et al. 2009. The B7 family member B7-H6 is a tumor cell ligand for the activating natural killer cell receptor NKp30 in humans. *J. Exp. Med.* 206:1495–1503. doi:10.1084/jem.20090681

Bromley, S.K., W.R. Burack, K.G. Johnson, K. Somersalo, T.N. Sims, C. Sumen, M.M. Davis, A.S. Shaw, P.M. Allen, and M.L. Dustin. 2001. The immunological synapse. *Annu. Rev. Immunol.* 19:375–396. doi:10.1146/annurev.immunol.19.1.375

Brünger, A.T., P.D. Adams, G.M. Clore, W.L. DeLano, P. Gros, R.W. Grosse-Kunstleve, J.S. Jiang, J. Kuszewski, M. Nilges, N.S. Pannu, et al. 1998. Crystallography & NMR system: a new software suite for macromolecular structure determination. *Acta Crystallogr. D Biol. Crystallogr.* 54:905–921. doi:10.1107/S0907444998003254

Bryceson, Y.T., and E.O. Long. 2008. Line of attack: NK cell specificity and integration of signals. *Curr. Opin. Immunol.* 20:344–352. doi:10.1016/j.coi.2008.03.005

Bryceson, Y.T., M.E. March, H.G. Ljunggren, and E.O. Long. 2006. Activation, coactivation, and costimulation of resting human natural killer cells. *Immunol. Rev.* 214:73–91. doi:10.1111/j.1600-065X.2006.00457.x

Cantoni, C., M. Ponassi, R. Biassoni, R. Conte, A. Spallarossa, A. Moretta, L. Moretta, M. Bolognesi, and D. Bordo. 2003. The three-dimensional structure of the human NK cell receptor NKp44, a triggering partner in natural cytotoxicity. *Structure.* 11:725–734. doi:10.1016/S0969-2126(03)00095-9

Davis, D.M., I. Chiu, M. Fassett, G.B. Cohen, O. Mandelboim, and J.L. Strominger. 1999. The human natural killer cell immune synapse. *Proc. Natl. Acad. Sci. USA.* 96:15062–15067. doi:10.1073/pnas.96.26.15062

Deng, L., and R.A. Mariuzza. 2006. Structural basis for recognition of MHC and MHC-like ligands by natural killer cell receptors. *Semin. Immunol.* 18:159–166. doi:10.1016/j.smim.2006.03.004

Foster, C.E., M. Colonna, and P.D. Sun. 2003. Crystal structure of the human natural killer (NK) cell activating receptor NKp46 reveals structural relationship to other leukocyte receptor complex immunoreceptors. *J. Biol. Chem.* 278:46081–46086. doi:10.1074/jbc.M308491200

Ikemizu, S., R.J.C. Gilbert, J.A. Fennelly, A.V. Collins, K. Harlos, E.Y. Jones, D.I. Stuart, and S.J. Davis. 2000. Structure and dimerization of a soluble form of B7-1. *Immunity.* 12:51–60. doi:10.1016/S1074-7613(00)80158-2

Lanier, L.L. 2008. Up on the tightrope: natural killer cell activation and inhibition. *Nat. Immunol.* 9:495–502. doi:10.1038/ni1581

Larsen, C.P., T.C. Pearson, A.B. Adams, P. Tso, N. Shirasugi, E. Strobert, D. Anderson, S. Cowan, K. Price, J. Naemura, et al. 2005. Rational development of LEA29Y (belatacept), a high-affinity variant of CTLA4-Ig with potent immunosuppressive properties. *Am. J. Transplant.* 5:443–453. doi:10.1111/j.1600-6143.2005.00749.x

Laskowski, R.A., M.W. MacArthur, D.S. Moss, and J.M. Thornton. 1993. PROCHECK: A program to check the stereo chemical quality of protein structures. *J. Appl. Crystallogr.* 26:283–291. doi:10.1107/S0021889892009944

Lawrence, M.C., and P.M. Colman. 1993. Shape complementarity at protein/protein interfaces. *J. Mol. Biol.* 234:946–950. doi:10.1006/jmbi.1993.1648

Lázár-Molnár, E., Q. Yan, E. Cao, U. Ramagopal, S.G. Nathenson, and S.C. Almo. 2008. Crystal structure of the complex between programmed death-1 (PD-1) and its ligand PD-L2. *Proc. Natl. Acad. Sci. USA.* 105:10483–10488. doi:10.1073/pnas.0804453105

Li, P., D.L. Morris, B.E. Willcox, A. Steinle, T. Spies, and R.K. Strong. 2001. Complex structure of the activating immunoreceptor NKG2D and its MHC class I-like ligand MICA. *Nat. Immunol.* 2:443–451.

Li, P., G. McDermott, and R.K. Strong. 2002. Crystal structures of RAE-1β and its complex with the activating immunoreceptor NKG2D. *Immunity.* 16:77–86. doi:10.1016/S1074-7613(02)00258-3

Lin, D.Y., Y. Tanaka, M. Iwasaki, A.G. Gittis, H.-P. Su, B. Mikami, T. Okazaki, T. Honjo, N. Minato, and D.N. Garboczi. 2008. The PD-1/PD-L1 complex resembles the antigen-binding Fv domains of antibodies and T cell receptors. *Proc. Natl. Acad. Sci. USA.* 105:3011–3016. doi:10.1073/pnas.0712278105

Lo Conte, L., C. Chothia, and J. Janin. 1999. The atomic structure of protein-protein recognition sites. *J. Mol. Biol.* 285:2177–2198. doi:10.1006/jmbi.1998.2439

McCann, F.E., P. Eissmann, B. Onfelt, R. Leung, and D.M. Davis. 2007. The activating NKG2D ligand MHC class I-related chain A transfers from target cells to NK cells in a manner that allows functional consequences. *J. Immunol.* 178:3418–3426.

McFarland, B.J., T. Kortemme, S.F. Yu, D. Baker, and R.K. Strong. 2003. Symmetry recognizing asymmetry: analysis of the interactions between the C-type lectin-like immunoreceptor NKG2D and MHC class I-like ligands. *Structure.* 11:411–422. doi:10.1016/S0969-2126(03)00047-9

McRee, D.E. 1999. XtalView/Xfit—A versatile program for manipulating atomic coordinates and electron density. *J. Struct. Biol.* 125:156–165. doi:10.1006/jsbi.1999.4094

Moretta, A., C. Bottino, M. Vitale, D. Pende, C. Cantoni, M.C. Mingari, R. Biassoni, and L. Moretta. 2001. Activating receptors and coreceptors involved in human natural killer cell-mediated cytolysis. *Annu. Rev. Immunol.* 19:197–223. doi:10.1146/annurev.immunol.19.1.197

Moretta, L., C. Bottino, D. Pende, R. Castriconi, M.C. Mingari, and A. Moretta. 2006. Surface NK receptors and their ligands on tumor cells. *Semin. Immunol.* 18:151–158. doi:10.1016/j.smim.2006.03.002

Natarajan, K., N. Dimasi, J. Wang, R.A. Mariuzza, and D.H. Margulies. 2002. Structure and function of natural killer cell receptors: multiple molecular solutions to self, nonself discrimination. *Annu. Rev. Immunol.* 20:853–885. doi:10.1146/annurev.immunol.20.100301.064812

Orange, J.S. 2008. Formation and function of the lytic NK-cell immunological synapse. *Nat. Rev. Immunol.* 8:713–725. doi:10.1038/nri2381

Otwinowski, Z., and W. Minor. 1997. Processing of X-ray diffraction data collected in oscillation mode. *Methods Enzymol.* 276:307–326. doi:10.1016/S0076-6879(97)76066-X

Pende, D., S. Parolini, A. Pessino, S. Sivori, R. Augugliaro, L. Morelli, E. Marcenaro, L. Accame, A. Malaspina, R. Biassoni, et al. 1999. Identification and molecular characterization of NKp30, a novel triggering receptor involved in natural cytotoxicity mediated by human natural killer cells. *J. Exp. Med.* 190:1505–1516. doi:10.1084/jem.190.10.1505

Pogge von Strandmann, E., V.R. Simhadri, B. von Tresckow, S. Sasse, K.S. Reiners, H.P. Hansen, A. Rothe, B. Böll, V.L. Simhadri, P. Borchmann, et al. 2007. Human leukocyte antigen-B-associated transcript 3 is released from tumor cells and engages the NKp30 receptor on natural killer cells. *Immunity.* 27:965–974. doi:10.1016/j.immuni.2007.10.010

Radaev, S., B. Rostro, A.G. Brooks, M. Colonna, and P. Sun. 2001. Conformational plasticity revealed by the cocrystal structure of NKG2D and its class I MHC-like ligand ULBP3. *Immunity.* 15:1039–1049. doi:10.1016/S1074-7613(01)00241-2

Raulet, D.H. 2003. Roles of the NKG2D immunoreceptor and its ligands. *Nat. Rev. Immunol.* 3:781–790. doi:10.1038/nri1199

Sasaki, T., E.C. Gan, A. Wakeham, S. Kornbluth, T.W. Mak, and H. Okada. 2007. HLA-B-associated transcript 3 (Bat3)/Scythe is essential for p300-mediated acetylation of p53. *Genes Dev.* 21:848–861. doi:10.1101/gad.1534107

Schwartz, J.-C.D., X. Zhang, A.A. Fedorov, S.G. Nathenson, and S.C. Almo. 2001. Structural basis for co-stimulation by the human CTLA-4/B7-2 complex. *Nature.* 410:604–608. doi:10.1038/35069112

Snanoudj, R., C. Frangié, B. Deroure, H. François, C. Créput, S. Beaudreuil, A. Dürrbach, and B. Charpentier. 2007. The blockade of T-cell co-stimulation as a therapeutic stratagem for immunosuppression: Focus on belatacept. *Biologics.* 1:203–213.

Soriani, A., A. Zingoni, C. Cerboni, M.L. Iannitto, M.R. Ricciardi, V. Di Gialleonardo, M. Cippitelli, C. Fionda, M.T. Petrucci, A. Guarini, et al. 2009. ATM-ATR-dependent up-regulation of DNAM-1 and NKG2D ligands on multiple myeloma cells by therapeutic agents results in enhanced

NK-cell susceptibility and is associated with a senescent phenotype. *Blood*. 113:3503–3511. doi:10.1182/blood-2008-08-173914

Stamper, C.C., Y. Zhang, J.F. Tobin, D.V. Erbe, S. Ikemizu, S.J. Davis, M.L. Stahl, J. Seehra, W.S. Somers, and L. Mosyak. 2001. Crystal structure of the B7-1/CTLA-4 complex that inhibits human immune responses. *Nature*. 410:608–611. doi:10.1038/35069118

Storoni, L.C., A.J. McCoy, and R.J. Read. 2004. Likelihood-enhanced fast rotation functions. *Acta Crystallogr. D Biol. Crystallogr.* 60:432–438. doi:10.1107/S0907444903028956

van der Merwe, P.A., D.L. Bodian, S. Daenke, P. Linsley, and S.J. Davis. 1997. CD80 (B7-1) binds both CD28 and CTLA-4 with a low affinity and very fast kinetics. *J. Exp. Med.* 185:393–403. doi:10.1084/jem.185.3.393

van der Merwe, P.A., S.J. Davis, A.S. Shaw, and M.L. Dustin. 2000. Cytoskeletal polarization and redistribution of cell-surface molecules during T cell antigen recognition. *Semin. Immunol.* 12:5–21. doi:10.1006/smim.2000.0203

Vyas, Y.M., H. Maniar, and B. Dupont. 2002. Visualization of signaling pathways and cortical cytoskeleton in cytolytic and noncytolytic natural killer cell immune synapses. *Immunol. Rev.* 189:161–178. doi:10.1034/j.1600-065X.2002.18914.x

Wang, J.H., A. Smolyar, K. Tan, J.H. Liu, M. Kim, Z.Y. Sun, G. Wagner, and E.L. Reinherz. 1999. Structure of a heterophilic adhesion complex between the human CD2 and CD58 (LFA-3) counterreceptors. *Cell*. 97:791–803. doi:10.1016/S0092-8674(00)80790-4

Williams, A.F., and A.N. Barclay. 1988. The immunoglobulin superfamily—domains for cell surface recognition. *Annu. Rev. Immunol.* 6:381–405. doi:10.1146/annurev.iy.06.040188.002121

Yokoyama, W.M., and B.F.M. Plougastel. 2003. Immune functions encoded by the natural killer gene complex. *Nat. Rev. Immunol.* 3:304–316. doi:10.1038/nri1055

Zou, W., and L. Chen. 2008. Inhibitory B7-family molecules in the tumour microenvironment. *Nat. Rev. Immunol.* 8:467–477. doi:10.1038/nri2326